Chemical Science

ROYAL SOCIETY OF CHEMISTRY

EDGE ARTICLE

View Article Online
View Journal | View Issue

Cite this: *Chem. Sci.*, 2024, **15**, 12459

All publication charges for this article have been paid for by the Royal Society of Chemistry

Received 12th March 2024
Accepted 16th June 2024

DOI: 10.1039/d4sc01695e

rsc.li/chemical-science

Key-to-lock halogen bond-based tetragonal pyramidal association of iodonium cations with the lacune rims of beta-octamolybdate†

Natalia S. Soldatova, [a] Amirbek D. Radzhabov, [a] Daniil M. Ivanov, [ab] Sergi Burguera, [c] Antonio Frontera, [c] Pavel A. Abramov, *[ad] Pavel S. Postnikov *[ae] and Vadim Yu. Kukushkin *[bf]

The structure-directing "key-to-lock" interaction of double σ-(I^{III})-hole donating iodonium cations with the O-flanked pseudo-lacune rims of $[\beta\text{-}Mo_8O_{26}]^{4-}$ gives halogen-bonded iodonium-beta-octamolybate supramolecular associates. In the occurrence of their tetragonal pyramidal motifs, deep and broad σ-(I^{III})-holes of a cation recognize the molybdate backbone, which provides an electronic pool localized around the two lacunae. The halogen-bonded I···O linkages in the structures were thoroughly studied computationally and classified as two-center, three-center bifurcated, and unconventional "orthogonal" I···O halogen bonds. In the latter, the O-atom approaches orthogonally the C–I^{III}–C plane of an iodonium cation and this geometry diverge from the IUPAC criteria for the identification of the halogen bond.

1. Introduction

The specific molecular recognition represents an important driving force of a great number of processes spanning from supramolecular chemistry to biology and medicinal chemistry.[1–8] The recognition parameters between "key" and "lock", such as geometry, size, type of interactions and their number, are the main points to achieve proper conditions for the supramolecular assembly.[9] In terms of bonding between coformers, the recognition pathway could involve a number of energetically differentiated steps. Inside this energetically scaled pool, noncovalent interactions (abbreviated as NCIs; for general reviews on NCIs see ref. 10–17) play a structure-directing role for various supramolecular associations or recognition processes between the "key" and "lock" coformers to accomplish, *e.g.* host–guest complexes[18] or clathrates.[19] A special attention, in this context, has been drawn to the utilization of polynuclear transition metal oxocomplexes (polyoxometalates, POM; for reviews on POMs see ref. 20–25) as building blocks for the design of new smart materials for energy conversion, storage and transfer systems.[26–32] Despite the wide applicability of POMs, their involvement in "key-to-lock" recognition systems is poorly studied. A rare example, for instance, demonstrates site-specific anchoring of organo-boronic acids to the metal-functionalized Dawson anions $[M_3P_2W_{15}O_{62}]^{9-}$ (M = Ta, Nb).[33]

In view of our interest in applications of a particular class of POMs, namely polyoxomolybdates (for recent relevant studies see ref. 34–39), we[40–44] and other groups[45–47] previously employed these species as receptors in the recognition systems. In the chemistry of polyoxomolybdates, the $[\beta\text{-}Mo_8O_{26}]^{4-}$ anion is a widely used tecton for crystal engineering and design of new compounds;[38,48–53] it contains two lacunae that can function as "locks" for various electrophilic "keys" (Fig. 1A).

Particularly, we reported on the employment of beta-octamolybdate anion (Fig. 1) as a ligand or "lock" for Ag^+, which function as "key".[40–42] This "key-to-lock" recognition was achieved due to the presence of two pseudo-lacunae, in the structure of the POM anion. These lacunae of the $[\beta\text{-}Mo_8O_{26}]^{4-}$ anion also exhibited an ability to interact with hydrogen bond (abbreviated as HB) donors, like O–H, N–H, or even C–H groups – all acting as electrophilic coformers of NCIs.[43] The ability of the lacunae to function as HB acceptor in the "key-to-lock" recognition stimulated our further studies focused on the employment of $[\beta\text{-}Mo_8O_{26}]^{4-}$ as nucleophilic partner toward such unconventional types of NCIs (sometimes refereed to unorthodox[54,55] or exotic[56]) as halogen bonding (abbreviated as XB). According to with the IUPAC definition of XB,[57] "a halogen

[a]*Research School of Chemistry and Applied Biomedical Sciences, Tomsk Polytechnic University, Tomsk 634050, Russian Federation. E-mail: postnikov@tpu.ru*

[b]*Institute of Chemistry, Saint Petersburg State University, Universitetskaya Nab. 7/9, Saint Petersburg 199034, Russian Federation. E-mail: v.kukushkin@spbu.ru*

[c]*Department of Chemistry, Universitat de les Illes Balears, Crta. de Valldemossa km 7.5, Palma de Mallorca (Baleares) 07122, Spain*

[d]*Nikolaev Institute of Inorganic Chemistry SB RAS, 3 Acad. Lavrentiev Av., Novosibirsk 630090, Russian Federation. E-mail: abramov@niic.nsc.ru*

[e]*Department of Solid State Engineering, University of Chemical Technology, Prague 16628, Czech Republic*

[f]*Institute of Chemistry and Pharmaceutical Technologies, Altai State University, Barnaul 656049, Russian Federation*

† Electronic supplementary information (ESI) available. CCDC 2334360–2334364. For ESI and crystallographic data in CIF or other electronic format see DOI: https://doi.org/10.1039/d4sc01695e

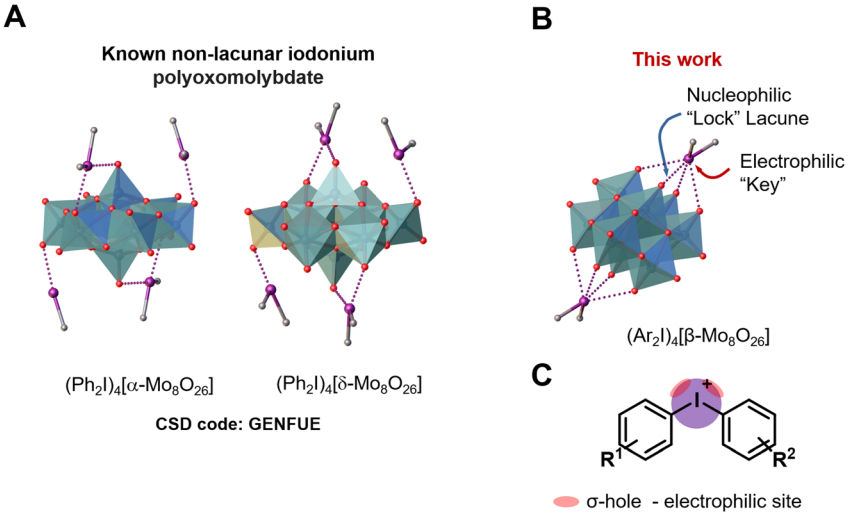

Fig. 1 Structure of the iodonium α- and δ-octamolybdate (A); structure of $[\beta\text{-}Mo_8O_{26}]^{4-}$ anion (B) and graphical representation of iodonium cations highlighting σ-holes (C).

bond… is a net attractive interaction between an electrophilic region associated with a halogen atom in a molecular entity and a nucleophilic region in another, or the same, molecular entity". For general reviews on XB see ref. 58–62.

Among various NCIs, XB can be considered as one of the most suitable alternatives to HB for NCI-involving crystal engineering. It is well-documented[58,59,63–65] that XB is significantly more directional force than HB and this structure-determining property has been actively used in the targeted construction of XB-based linear or orthogonal assemblies.[58] In the vast majority of studies, monovalent halogen-containing organic compounds were implemented as XB donors.[66] A relatively new trend in XB-involving crystal engineering and catalysis (explored mostly by Resnati,[62,67] Huber,[68–71] and some of us, see ref. 72–74 and references therein) is the utilization of hypervalent iodine compounds, particularly iodonium salts,[75] where I^{III} sites function as efficient double σ-hole donors[76] (biaxial σ-hole donors in another terminology;[68] Fig. 1B). Cationic nature of these iodonium species allows the rational design of new supramolecular architectures[72–74] based on charge-supported XB that is conventionally stronger than XB, which is associated with coformers featuring a iodine(I) site. Thus, iodonium cations can function as a close-to-perfect "key" toward a lacune of POM which act as a "lock". Notably, examples of nonlacunar iodonium POMs (*e.g.*, $[\alpha\text{- and }\delta\text{-}Mo_8O_{26}]^{4-}$)[77] were reported (Fig. 1B). In contrast to the lacunar $[\beta\text{-}Mo_8O_{26}]^{4-}$, the assemblies do not include any specified site of $[\alpha\text{- and }\delta\text{-}Mo_8O_{26}]^{4-}$ that will be bound to iodine(III) center.

In line with the previous studies focused on the $[\beta\text{-}Mo_8O_{26}]^{4-}$-based recognition systems utilizing $H\cdots O_{POM}$[43,78–81] and $Ag^{I}\cdots O_{POM}$[40–42] bonding, we now report on the structure-directing "key-to-lock" XB-involving interaction of double σ-hole donating iodonium cations with the lacune rims of $[\beta\text{-}Mo_8O_{26}]^{4-}$ to give halogen-bonded supramolecular associates. In the occurrence of these assemblies, deep and broad σ-(I^{III})-holes of the cation recognize the molybdate backbone which provides an electronic pool localized around the two lacunae.

2. Results and discussion

2.1. Halogen-bonded POMs

In overwhelming majority of the solid halogen-bonded POMs, monovalent halogen-containing compounds were used as XB donors,[44,82–86] while pairing between POMs and iodonium salts, exhibiting double σ-(I^{III})-hole site, is very little studied and only two relevant reports appeared in the literature. The first one has been focused on UV induced polymerization, in which the added POMs assisted the generation of phenyl radicals from corresponding iodonium salts.[87–90] Although, the formed intermediate was isolated as the solid, it was not studied by single-crystal X-ray diffraction (SCXRD) and, consequently, its structure was not reliably established. In the second study, $(Ph_2I)_4[\text{-}Mo_8O_{26}]\cdot 3DMF\cdot H_2O$ was used for the design of iodine-doped molybdenum carbide nanocomposite for an electrochemical hydrogen evolution reaction.[77] In the crystal structure of $(Ph_2\text{-}I)_4[Mo_8O_{26}]\cdot 3DMF\cdot H_2O$, α- and δ-isomers of the octamolybdate ion are bound to the iodonium cations *via* the O-atom of the Mo=O group. However, XB features (even unconventional orthogonal XBs; Section 2.3.4) in the crystal structure organization have not been discussed. Notably, α- and δ-isomers of $[Mo_8O_{26}]^{4-}$ do not contain "lock" lacunae to accept the "key" site of R_2I^+ and it seemed that the use of $[\beta\text{-}Mo_8O_{26}]^{4-}$ is a prerequisite for the targeted assembly. Our MEP surface calculation data for α, β, γ, and $\delta\text{-}[Mo_8O_{26}]^{4-}$ isomeric anions, clearly showing the availability of the lacunae in $[\beta\text{-}Mo_8O_{26}]^{4-}$ and their absence in α, γ, and δ-isomers, are given in the ESI.†

As electrophilic coformers for this study, we addressed diaryliodonium cations shown in Table 1. The corresponding iodonium salts are easy-to-hand stable substrates that can be prepared from elemental iodine, aromatic hydrocarbons, and such practical oxidant system as Oxone®-H_2SO_4.[91] The anion metathesis of these salts with $(n\text{-}Bu_4N)_4[\beta\text{-}Mo_8O_{26}]$ provides iodonium beta-octamolybdate associates detailed in the next section.

Table 1 Studied complexes **1–5**

Complex	Iodonium cation	Composition
1	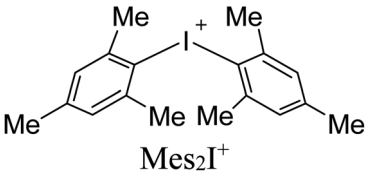 Mes_2I^+	$(Mes_2I)_4[Mo_8O_{26}]\cdot 2.6DMF$
2	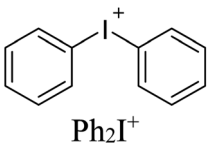 Ph_2I^+	$(Ph_2I)_4[Mo_8O_{26}]\cdot 2DMSO$
3		$(Ph_2I)_4[Mo_8O_{26}]\cdot 2DMF$
4	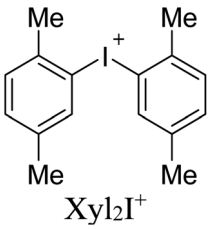 Xyl_2I^+	$(Xyl_2I)_2(n\text{-}Bu_4N)_2[Mo_8O_{26}]\cdot 1.7DMSO$
5		$(Xyl_2I)_2(n\text{-}Bu_4N)_2[Mo_8O_{26}]\cdot Et_2O$

2.2. Synthesis and structures

Associates **1–5** were obtained as the solid by a conventional[40,41,44] approach that includes vapor diffusion of Et_2O (**1**, **3**, **5**) or *i*-PrOH (**2**, **4**) into solutions of $(n\text{-}Bu_4N)_4[\beta\text{-}Mo_8O_{26}]$ in DMF (**1**, **3**,**5**) or DMSO (**2**, **4**) (Table 1); for synthetic details see Experimental section. Complexes **1–5** were studied by SCXRD; the phase purity of **1**, **2**, and **4** was confirmed by powder X-ray diffraction. The SCXRD structures of **3** and **5** are well-refined and suitable for the analysis of NCIs. It is noteworthy, however, that the crystals of **3** and **5** contained phase admixtures; all our attempts to isolate phase pure complexes failed.

Association mode of the iodonium cations with $[\beta\text{-}Mo_8O_{26}]^{4-}$ depends on the identity of Ar_2I^+. In the solid **1–3**, all $n\text{-}Bu_4N^+$ cations from the starting material were fully replaced by the iodonium cations, while the association involving Xyl_2I^+ gave the mixed $Xyl_2I^+/n\text{-}Bu_4N^+$ counter-ion system observed in the structures of **4** and **5** (Table 1). The complete replacement of the $n\text{-}Bu_4N^+$ cations in **4** and **5** was not achieved even with 4 equiv. of $(Xyl_2I)OTf$. Complex **2** contains two independent iodonium POM arrays, in the text referred to $\mathbf{2^I}$ and $\mathbf{2^{II}}$.

Crystal packings of **1–5** are shown in Fig. S8–S13 (Section S5, the ESI†). The contacts between corresponding cations and the anion include C–H···O_{POM} H-bonds (**1–5**), π–π interactions between iodonium cations (**2**, **3**), and C–H···π interactions (**1**, **2**, **4**, **5**).

2.3. NCIs with the lacune rims

2.3.1. General consideration. In the structures of **1–5**, two iodonium cations interact with two lacune rims of the polyoxomolybdate backbone *via* NCIs occurred between a I^{III} site and oxoligands (Fig. 2 and 3). The structures of **1–3** are involved in NCIs with two more iodonium cations with out-of-lacune oxoligands of the POM surface, while for **4** and **5** such interactions were not observed because of the incomplete replacement of $n\text{-}Bu_4N^+$ by the Ar_2I^+ cations (Fig. 3).

Geometric parameters of NCIs involving the iodine(III) centers are summarized in Table 2. Consideration of chalcogen bond involving DMSO in the structure of $\mathbf{2^{II}}$ is given in the ESI (Section S1†) as these NCIs are out of scope of this study.

In the structures of **1–3**, the I···O distances between an I-atom and all O-atoms of the lacune rim (namely, O1–O4) are smaller (2.74–3.44 Å) than the sum of Bondi vdW radii (Σ_{vdW} I + O = 3.50 Å; Table 2). The systems of NCIs occurred between any one of the iodonium cations as "key" and the lacune rims as "lock" exhibit tetragonal pyramidal arrangement (Fig. 2). Notably, the IUPAC distance criterion for identification of XB[57] is not obeyed for the I···O4 separation in the structure of **4** (Nc for I1···O4 = 1.01) and for the I···O3 and I···O4 contacts in **5** (Nc for I1···O3 = 1.13 and Nc for I1···O4 = 1.17). The structures of **4** and **5** are not tetragonal pyramidal, but can be considered as multi-center XB (three-center for **4** and four-center for **5**, Fig. 3).

Although the I···O distance fulfill the IUPAC criteria for XB,[57] some I···O contacts cannot be unambiguously attributed to XB because of significant deviations of some ∠C–I···O angles (up to 79°) from linearity (Table 2).

2.3.2. Two-center halogen bonds. Two-center XB (Fig. 4A) exhibit the conventional type of interaction between I-atom and atom of nucleophile along the extension of the C–I bond. In **1–5**, an average value of Nc for I···O two-center XBs is around 0.82, that is the lowest value in comparison with Nc values for the other types of NCIs with the lacune rim (Table 2) considered in Sections 2.3.3. and 2.3.4.

2.3.3. Three-center bifurcated halogen bonds. The deviation of ∠C–I···O from 180° (in our case, as small as 135°) can be related to the known[92,93] bifurcation of XB (Fig. 4B). Bifurcated three-center XB is rather rare type of XB involving interaction, which includes contacts of an electrophilic region with two nucleophilic atoms; we previously suggested a classification of bifurcated XB including iodonium species.[92] Attribution of NCIs to bifurcated was additionally confirmed by natural bond orbital (NBO) analysis which showed the interaction between the O-atoms and σ*(C–I) (see Section 2.5. DFT calculation and Section S3 of the ESI†). The bifurcated bonds feature the much longer distance I···O in comparison with two-center XB (Nc 0.90 *vs.* 0.82).

2.3.4. Unconventional halogen bonds. This unique type of NCIs occurs between the lacune rim and a I-atom (Fig. 4C). These types of XB interactions warrant more detailed comments. Specifically, when both ∠C–I···O angles are approximately 90°, these NCIs diverge from the IUPAC definition[57] of XB. In these cases, the nucleophilic O-atom approaches the iodine site orthogonally relative to the C–I–C plane, rather than aligning along the extension of a C–I bond (Fig. 5). While fulfilling the IUPAC distance criterion and exhibiting a bond critical point (refer to Sections 2.5. and S3 of the ESI†), these interactions do not obey the IUPAC angular criterion, which presupposes linearity among the three atoms involved in occurrence of XB.[57]

To describe these specific interactions, we adopted the term "orthogonal XB", which is used to facilitate a clearer

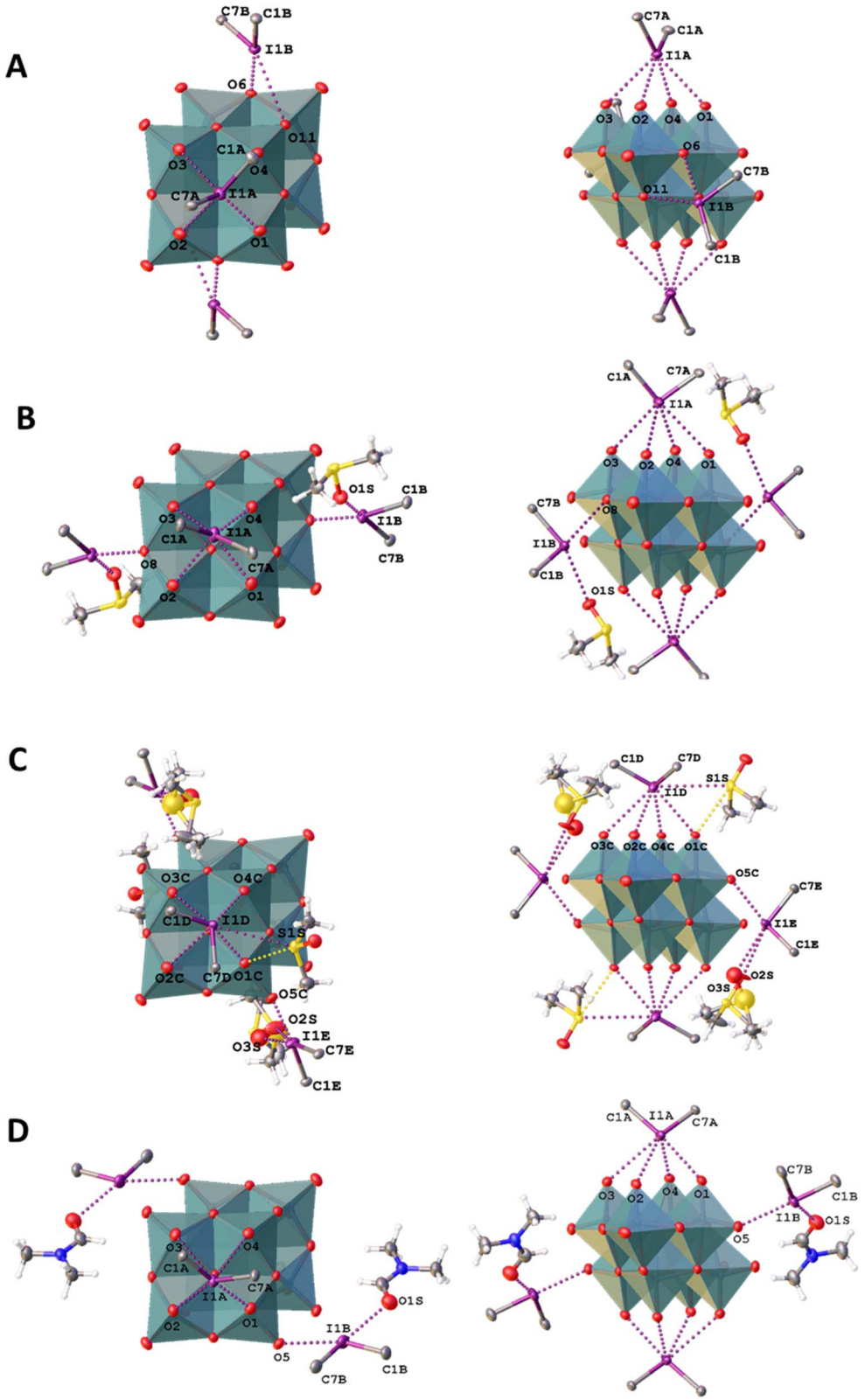

Fig. 2 XB-based linkage patterns of **1**–**3**: (A) **1**; (B) $\mathbf{2}^{I}$; (C) $\mathbf{2}^{II}$; (D) **3**.

understanding of these particular NCIs. The orthogonal XBs, as found in this study, do not involve interactions between the O-atoms and the σ*(C–I) orbital, signifying that these are not related to the σ-hole region of the I-atom. Notably, the average Nc value for the orthogonal XBs is 0.94, the highest among all XB types associated with the lacune rim. Based on this

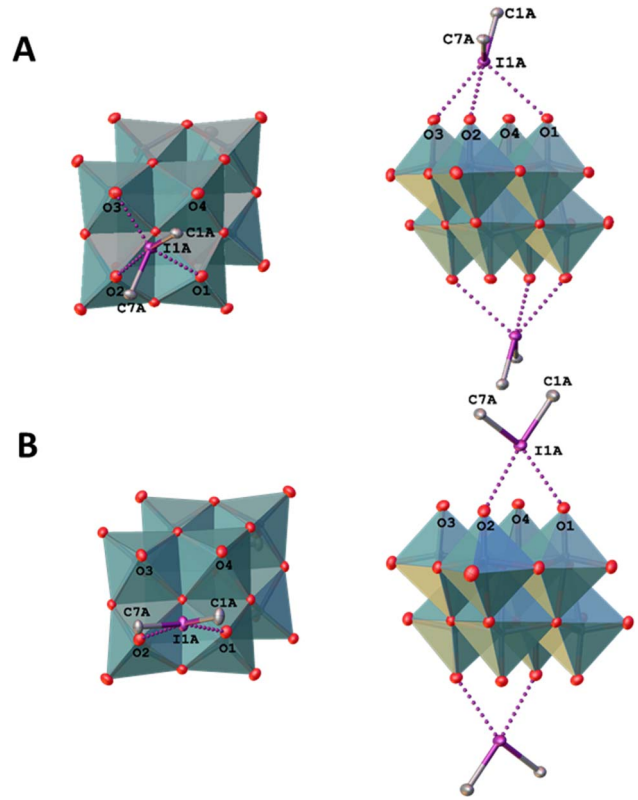

Fig. 3 XB-based structural arrays of **4** (A) and **5** (B).

classification, in the structures of **1–3**, at least one NCI with the lacune rim qualifies as an orthogonal XB (Table 2).

The molecular structure of compound **4** showcases a combination of two-center XB (I1···O2) and two orthogonal XBs (I1···O3 and I1···O2; Fig. 3). Interestingly, the IUPAC criteria for XB distance[57] are not fully met in certain interactions within this structure. Thus, the I···O4 separation in **4** (Nc 1.01) and the I···O3 and I···O4 contacts in **5** (Nc 1.13 and 1.17, respectively) do not align with the standard XB identification parameters.[57] Furthermore, our analysis of the structure of **5** confirmed the absence of orthogonal XB.

In certain instances, orthogonal XBs are observed to synergistically[93] coexist with hydrogen bonding[94] involving the O-atom of the POM and the *ortho*-H or *ortho*-CH_3 groups of the iodonium cation (Fig. 5). An extensive review of the CSD data, conforming to our classification criteria for the orthogonal XBs ($d(I\cdots O) < \Sigma_{vdW}$, ∠C–I···X 70–130°), revealed over 100 iodonium structures featuring the orthogonal XBs. Remarkably, only about a third of these structures exhibit a synergistic combination of orthogonal XB and HBs; this synergistic occurrence typically results in ∠C–I···X approaching 90°.

2.4. NCIs with out of the lacune rim oxo-ligands

In the structures of **1–3**, iodonium cations also interact with out of the lacune rim oxoligands (Fig. 2), while **4** and **5** do not display such interactions due to incomplete anion metathesis (Section 2.3.). For the structures of **1** and $\mathbf{2}^{I}$ XB involves the μ_2-O ligands, while for $\mathbf{2}^{II}$ and **3** the terminal Mo=O functionality functions as XB acceptor. All these I···O distances are smaller than Bondi Σ_{vdW} (3.50 Å; Nc = 0.76–0.92). Contacts with the bridging μ_2-O ligands are rather short (Nc 0.78 and 0.81) in comparison with XBs occurred between the I^{III} site and the Mo=O group (Nc 0.82 and 0.84). In addition, the structure of **1** exhibits NCI with the O-atom of the Mo–O–Mo linkage. The latter is characterized by a rather small Nc value (0.92) and low linearity (∠C7B–I1B···O11 = 134.39(10)°); this deviation is apparently caused by steric effects of iodonium cations and the anion. In **2–3**, the iodonium cations form XB with O-atoms out of the lacune rim and also O-atoms of the crystallization solvent (DMF or DMSO) and such I···O XBs are almost linear ∠C–I1···O = 161–171° (Table 3). Notably, all XBs with O-atoms of the solvent are shorter that XB with any oxo-ligands (Table 3); a similar situation was observed in the structures of the previously reported solvates of a iodonium cation with DMSO.[95,96]

2.5. DFT calculations

First, MEP surfaces of the cations and the anion were performed to rationalize the assemblies described above and the existence of multi-center XBs. The MEP surfaces of the cations are given in Fig. 6, showing the expected pair of σ-holes on each I-atom (marked with asterisks in Fig. 6) opposite to the I–C bonds. Their relative intensity behaves as expected considering the number of electron donor methyl groups, being the most positive ones those of the Ph_2I^+ moiety without additional Me-groups (Fig. 6b). Since the iodoniums are the cationic species, the MEP values are positive all over the van der Waals surface. However, an anisotropy of the electron density is observed at the I-atom with two regions where the MEP is less positive (local minima) above and below the C_2I plane (at the expected location of iodine's LPs).

The MEP surface of the anion is represented in Fig. 7, where the MEP values are very large and negative all over the van der Waals surface due to the tetra-anionic character of the polyoxometalate. Notably, it can be observed that the existence of two symmetrically equivalent MEP minima located at the lacune rim that is under the influence of four O-atoms (only one minimum is shown in Fig. 7). The maxima are located at two opposite vertices. This explains the occurrence of the tetragonal pyramidal arrangement, since the positive I-atom of the cation will tend to interact with the most negative part of the anion, under the effect of four O-atoms. Once two cations occupy the two minima, other regions with less negative MEP values are available, which are under the influence of three monocoordinated O-atoms, also in line with the occurrence of four-center XBs.

We analyzed neutral pentameric assemblies (the anion surrounded by four cations) of all compounds reported herein using a combination of QTAIM and NCIplot computational tools to study the contacts established between the cations and the anions. The assemblies of **1** and **3** are commented below (Fig. 8 and 9, respectively) and the rest are provided in the ESI (Fig. S4 and S5, Section S2 of the ESI†).

For the pentameric assembly of **1**, the QTAIM/NCIplot analysis evidences the existence of a multitude CH···O

Table 2 Geometric parameters of NCIs with the lacune rims in the structures of **1–5**[a,b]

Iodonium POM motif	Interactions with the lacune rim				NCI
	d(I1···O), Å/Nc[b]		∠(C–I1···O)		
1	O1	3.094(2)/0.88	C1	108.43(10)	
			C7	138.62(11)	bXB
	O2	3.050(3)/0.87	C1	162.58(7)	XB
			C7	98.7(1)	
	O3	3.257(2)/0.93	C1	103.02(11)	Orthogonal XB
			C7	113.93(8)	
	O4	3.1893(18)/0.91	C1	71.62(7)	
			C7	162.37(11)	bXB
2^{I}	O1	3.203(3)/0.92	C1	153.36(12)	bXB
			C7	81.27(11)	
	O2	3.238(2)/0.93	C1	104.50(14)	Orthogonal XB
			C7	121.25(9)	
	O3	2.999(3)/0.86	C1	98.94(14)	
			C7	166.10(14)	XB
	O4	3.036(3)/0.87	C1	146.62(12)	bXB
			C7	103.89(14)	
2^{II}	O1C	3.002(3)/0.86	C1	150.89(9)	XB
			C7	81.86(13)	
	O2C	3.4010(19)/0.97	C1	88.27(9)	Orthogonal XB
			C7	84.26(9)	
	O3C	3.260(3)/0.93	C1	76.19(12)	
			C7	141.34(9)	bXB
	O4C	3.135(3)0.90	C1	124.83(14)	
			C7	139.71(13)	bXB
3	O1	2.742(3)/0.78	C1	172.5(2)	XB
			C7	85.42(15)	
	O2	2.927(4)/0.84	C1	106.16(15)	
			C7	154.21(14)	XB
	O3	3.435(5)/0.98	C1	79.8(2)	Orthogonal XB
			C7	133.22(16)	
	O4	3.324(4)/0.95	C1	111.29(16)	Orthogonal XB
			C7	84.03(17)	
4	O1	3.2360(11)/0.92	C1	115.20(5)	Orthogonal XB
			C7	103.64(6)	
	O2	2.7382(13)/0.78	C1	171.54(7)	XB
			C7	79.17(6)	
	O3	3.2075(16)/0.92	C1	124.53(7)	Orthogonal XB
			C7	130.48(6)	
	O4	3.5413(14)/1.01	C1	98.88(6)	
			C7	158.11(6)	
5	O1	2.805(2)/0.80	C1	104.5(1)	
			C7	159.23(10)	XB
	O2	2.758(2)/0.79	C1	174.80(12)	XB
			C7	87.36(10)	
	O3	3.940(2)/1.13	C1	130.97(11)	
			C7	95.16(10)	
	O4	4.089(2)/1.17	C1	100.12(9)	
			C7	135.46(9)	

[a] The following color code is used in table: purple (two-center XB), blue (bifurcated XB; bXB), and green (orthogonal XB). [b] The normalized contact (Nc) is defined as the ratio between the separation observed in the crystal and the sum of Bondi vdW radii of interacting atoms: $Nc = d/\Sigma_{vdW}$; Σ_{vdW} I + O = 3.50 Å.

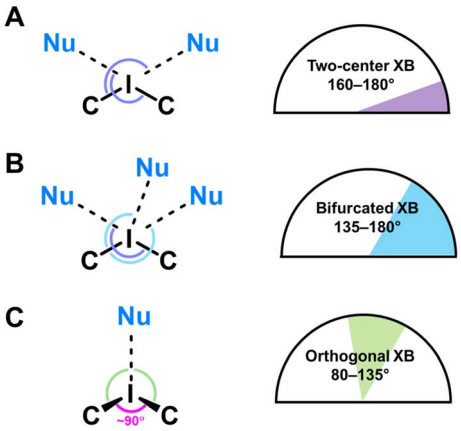

Fig. 4 Classification of the NCIs in 1–5. (A) Two-center XB; (B) bifurcated XB; (C) orthogonal XB.

contacts formed due to the electron-donating effect of the methyl substituents. Each contact is characterized by a bond critical point (BCP) and bond path connecting the H and O-atoms. The XBs are highlighted at the bottom of the Fig. 8 where the ancillary CH···O were omitted for the sake of clarity. It can be observed that for one pair of cations, the I-atom is linked to four O-atoms of the anion, establishing a tetragonal pyramidal assembly. This agrees well with the MEP analysis, since this iodine is located at the MEP minimum of the anion, thus maximizing the electrostatic attraction. Each XB is characterized by a BCP, bond path and green reduced density gradient (RDG) isosurface, thus disclosing the attractive nature of these XB contacts. For the other pair of cations, the I-atom is connected to three O-atoms of the anion by three BCPs and bond paths. By examining the color of the RDG isosurfaces, it can be deduced that in this case one of the XBs is stronger (blue isosurface) than the other two (green isosurface), also in agreement with the geometric features of the XBs (Section 2.3.).

The formation energy of this pentameric assembly is very large (-836.7 kcal mol^{-1}) due to the pure coulombic attraction between a tetra-anionic species and four surrounding cations. In this case, it is more convenient to discuss the energetic features of the assemblies using the interaction energies derived from the QTAIM analysis (using the V_b values), since they are free from the influence of pure electrostatic effects. The energetic contribution of all CH···O contacts observed in the pentamer is indicated in Fig. 8 (see also Table 4). This contribution is quite significant (-16.1 kcal mol^{-1}) due to the presence of numerous CH···O contacts. The contribution of the XBs is also indicated in Fig. 8 and it is much larger (-53.4 kcal mol^{-1}), evidencing that it is the dominant interaction. The individual energies of the XBs are indicated in blue close to the BCPs that characterize the XBs. It is interesting to emphasize that for the XB in the tetragonal pyramidal arrangement, all energies are similar (ranging -2.5 to -3.6 kcal mol^{-1}), thus suggesting that the location of the I-atom in this cation is likely dominated by the nondirectional electrostatic attraction. However, in the other binding mode (four-center XBs), one XB is very strong and directional

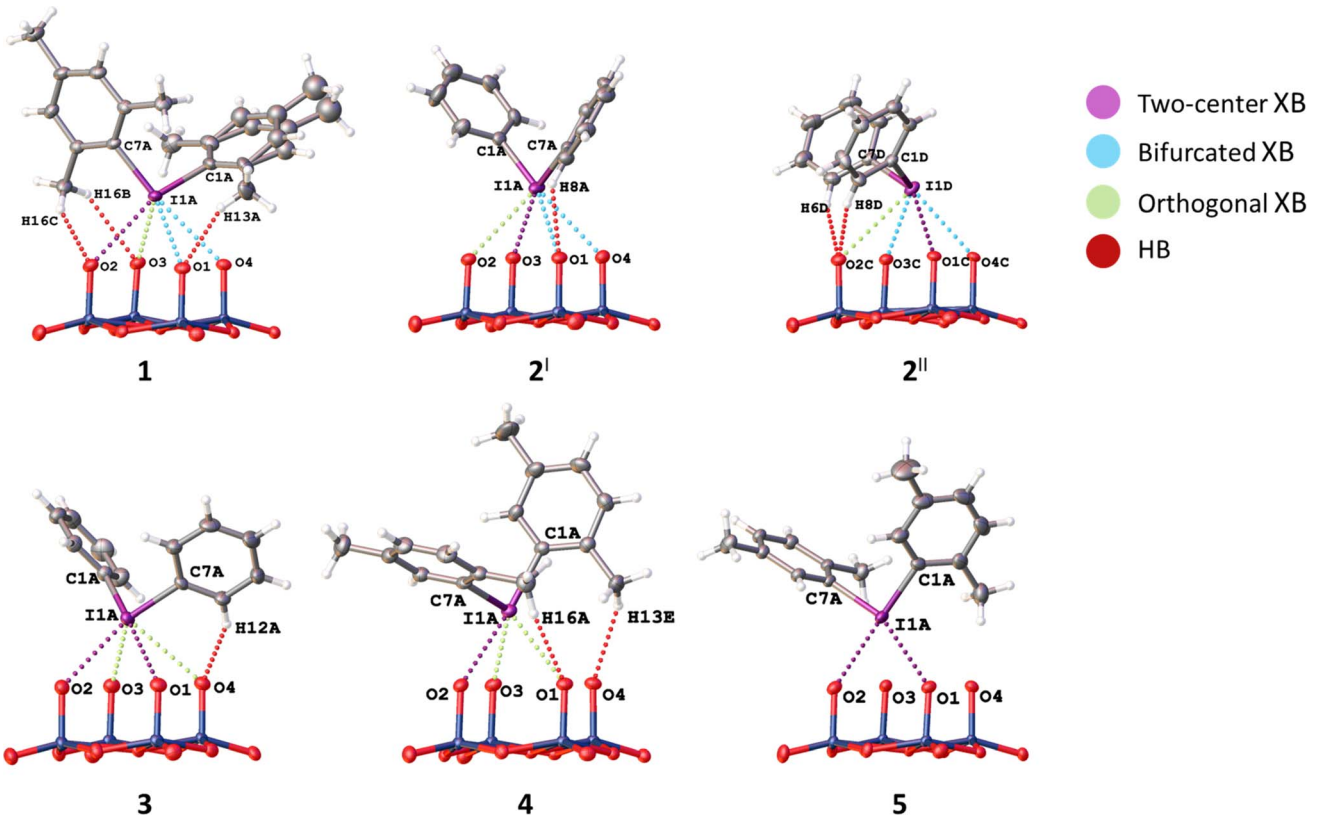

Fig. 5 Classified NCIs with lacune rims in 1–5.

Table 3 Observed XBs in the structures of **1–3**

Iodonium POM motif	XB	d(C–I···O), Å/Nc[a]	∠(C–I1···O), °
1	C1B–I1B···O6	2.733(2)/0.78	174.14(9)
	C7B–I1B···O11	3.237(3)/0.92	134.39(10)
$\mathbf{2}^{\mathrm{I}}$	C1B–I1B···O8	2.838(3)/0.81	162.57(14)
	C7B–I1B···O1S	2.745(3)/0.78	161.80(13)
$\mathbf{2}^{\mathrm{II}}$	C1E–I1E···O5C	2.855(3)/0.82	169.87(14)
	C7E–I1E···O2S	2.646(5)/0.76	163.25(16)
	C7E–I1E···O3S	2.783(15)/0.80	171.2(4)
3	C1B–I1B···O5	2.956(4)/0.84	164.51(17)
	C7B–I1B···O1S	2.830(5)/0.81	161.2(2)

[a] The normalized contact (Nc) is defined as the ratio between the separation observed in the crystal and the sum of Bondi vdW radii of interacting atoms: Nc = d/Σ_{vdW}; Σ_{vdW} I + O = 3.50 Å

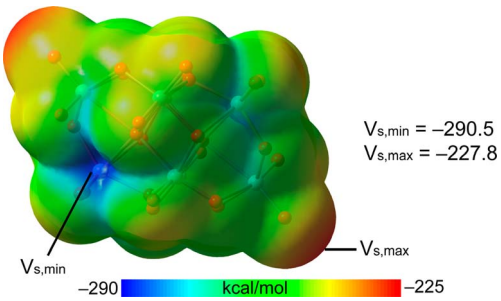

Fig. 7 MEP surface (isodensity 0.001 a.u.) of β-$[Mo_8O_{26}]^{4-}$. The MEP maximum, minimum values are given in kcal mol^{-1}.

(−9.1 kcal mol^{-1}) and the other two are much weaker ancillary XBs. Hence, in this case the directional XB dominates over the effect of the simple electrostatic attraction.

A parallel analysis for **3** is provided in Fig. 9, where the main difference with **1** is the reduced number of CH···O contacts due to the absence of methyl groups. In case of the XBs, the main difference with **1** is that in one pair of symmetrically equivalent cations, the I-atoms form three-center XBs instead of four-center XB. Therefore, the total contribution of the I···O contacts is smaller in **3**. For the tetragonal pyramidal arrangement that is highlighted in the bottom part of Fig. 9 there are two XBs that are clearly stronger than the other two. This is not observed in **1** and a likely explanation is that in **3** a better adjustment of the geometry of the cation on the surface of the anion is possible due to the absence of the CH_3···O contacts, facilitating the occurrence of more directional and shorter XBs.

The energetic and QTAIM/NCIplot analyses of **2**, **4**, and **5** are given in the ESI,† disclosing similar results. Moreover, the energetic results for all compounds are summarized in Table 4, evidencing that in **1–3** the XB is more relevant than the HB. In the cases of **4** and **5**, since two cations of the pentameric assemblies are tetrabutylammonium cations instead of iodonium cations, the contribution of CH···O interactions significantly increases and that of the I···O XBs decreases. For **4** and **5**, the energies given in parenthesis in the E_{HB} column correspond to the CH···O contribution of the Xyl_2I^+ cations. It can be observed that it is smaller than half of E_{HB} of **1** but larger than half of E_{HB} in **2** and **3**, in line with the absence of methyl groups in the latter two compounds.

The natural bond orbital (NBO) analysis of the assemblies under consideration was performed to verify the orbitals involved in the donor–acceptor interactions and to confirm the σ-hole nature of the XB contacts by the implication of the antibonding σ*(C–I) orbital. The results for **1** and **3** are shown in Fig. 10 and 11 and those of **2**, **4**, and **5** in the ESI (Fig. S6 and S7†). In the case of **1**, for the tetragonal pyramidal binding mode (Fig. 10a and b), we observed the electron donation from LPs located at three O-atoms of the anion to the antibonding σ*(C–I) orbitals of the cation. The I···O contact of the tetragonal

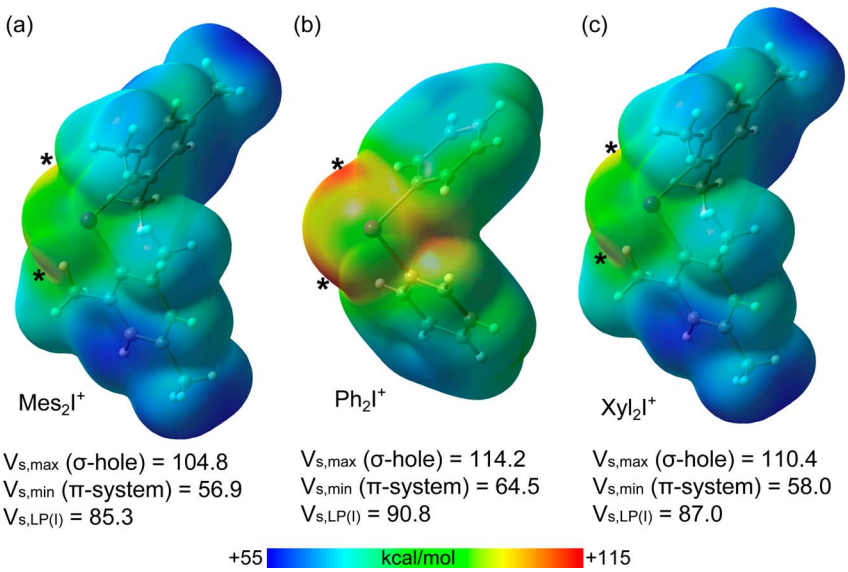

Fig. 6 MEP surfaces (isodensity 0.001 a.u.) of Mes_2I^+ (a), Ph_2I^+ (b), and Xyl_2I^+ (c). The MEP maximum, minimum values are given in kcal mol^{-1}. Moreover, the MEP values at the local minimum located over the I-atom are also indicated ($V_{s,LP(I)}$) in kcal mol^{-1}.

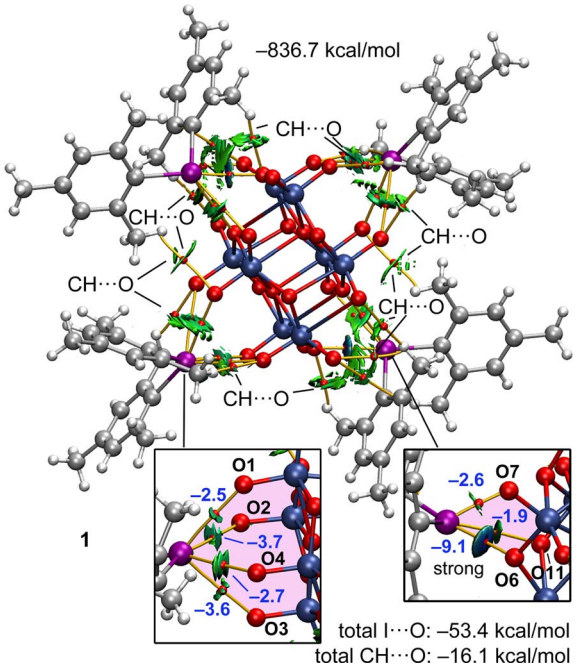

Fig. 8 Combined QTAIM (BCPs in red and bond path as solid orange lines) and NCIplot analysis (RDG = 0.5, $\rho_{cut\text{-}off}$ = 0.04, color range −0.04 a.u. ≤ (signλ_2)*ρ ≤ 0.04 a.u. of the pentameric assembly of **1**. The interaction energy is also indicated. The total contributions of the CH···O and I···O derived from the V_b values are indicated. Moreover, the individual contributions of the XBs are indicated in blue adjacent to the BCPs. Only intermolecular interactions are represented.

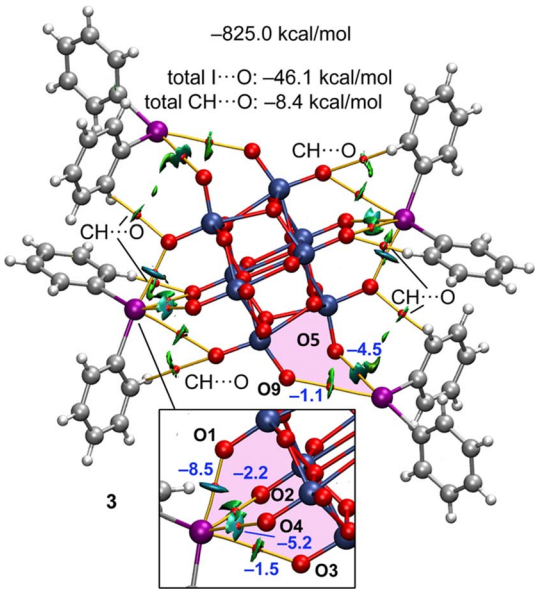

Fig. 9 Combined QTAIM (BCPs in red and bond path as solid orange lines) and NCIplot analysis (RDG = 0.5, $\rho_{cut\text{-}off}$ = 0.04, color range −0.04 a.u. ≤ (signλ_2)*ρ ≤ 0.04 a.u. of the pentameric assembly of **3**. The interaction energy is also indicated. The total contributions of the CH···O and I···O derived from the V_b values are indicated. Moreover, the individual contributions of the XBs are indicated in blue adjacent to the BCPs. Only intermolecular interactions are represented.

Table 4 Total formation energies (E), contribution of CH···O (E_{HB}) and I···O (E_{XB}) for **1–5** in kcal mol^{-1}. In parenthesis we give the values of the HB coming from the Xyl_2I^+ contacts (not considering the tetrabutylammonium HB with the POM); see Section 4.5. for details

Compound	E	E_{HB}	E_{XB}
1	−836.7	−16.1	−52.2
2	−816.3	−6.7	−38.6
3	−825.0	−8.4	−46.0
4	−837.6	−32.3 (−5.6)	−29.4
5	−822.2	−26.7 (−5.0)	−31.6

pyramidal binding mode that does not exhibit orbital mediated charge transfer corresponds to the longest I···O contact, where the overlap of the orbitals is likely too small (smaller than the threshold used by the program). In any case, the fact that, for three out of four contacts, the LP(O) → σ*(C–I) charge transfer is observed strongly suggests the σ-hole nature of the interaction. In the case of the four-center interaction (Fig. 10c), the NBO discloses the existence of a single LP(O) → σ*(C–I) charge transfer that corresponds to the strongest XB, in line with the QTAIM/NCIplot analysis data.

The NBOs corresponding to the XBs in **3** are given in Fig. 11. As also observed in **1**, for the tetragonal pyramidal assembly, three LP(O) → σ*(C–I) donor–acceptor interactions are observed and for the three-center XB only one, corresponding to the strongest and more directional XB. No other orbital donor–acceptor interactions were identified, thus confirming that only the antibonding σ*(C–I) orbital of the cation is involved in the binding mechanism. The results for **2**, **4**, and **5** (the ESI†) demonstrate a similar behavior.

3. Conclusions

The results of this study can be considered from at least two main perspectives. Firstly, we observed that iodonium cations interact with the lacune rim of the beta-octamolybate anion, [β-Mo_8O_{26}]$^{4-}$, to form halogen-bonded assemblies, exhibiting the tetragonal pyramidal motif. This association belongs to the "key-to-lock" category (as it was defined by Lehn[9]) when the I^{III}-site recognizes O-atoms of the rim, namely deep and broad σ-(I^{III})-holes of the cation interact with the molybdate backbone which provides an electronic pool localized around two pseudo-cavities. The iodonium cation acts as a "key", and the anion acts as a "lock": these partners form "well-defined noncovalent interaction, geometrical and interactional complementarity and energy gain".[9] It is noteworthy that α- and δ-[Mo_8O_{26}]$^{4-}$ do not exhibit "lock" lacunae to accept the "key" R_2I^+ and the use of the lacunar cluster [β-Mo_8O_{26}]$^{4-}$ is a prerequisite for the XB-based assembly.

In a broader sense, we found a novel type of supramolecular organization of POMs, which is based on XB. Consideration of the previous data on hydrogen-bond[43,78–81] and silver(I)[40–42] recognitions of the O-flanked lacune of beta-octamolybate and also this study focused on XB-involving assembly – all together – give a hint that similar recognition for the targeted

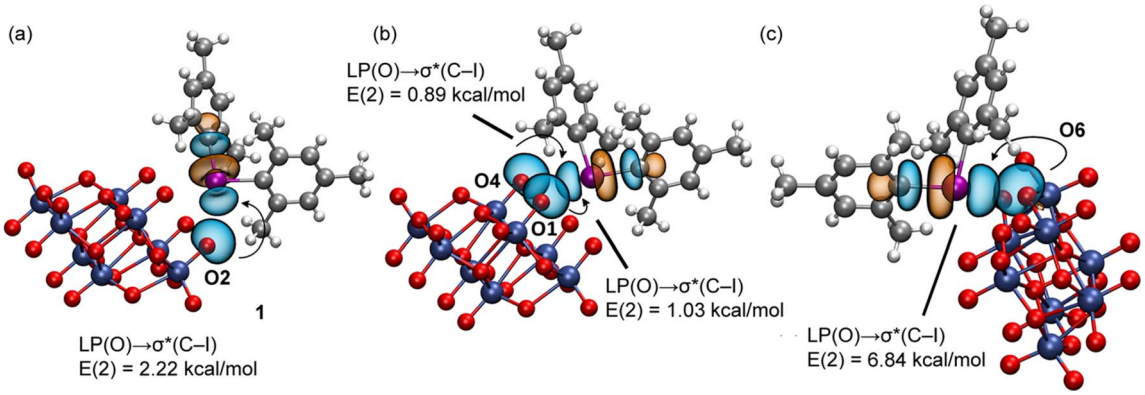

Fig. 10 NBOs involved in the XBs observed in **1** for the tetragonal pyramidal (a and b) and four-center (c) binding modes. The second order perturbation analysis energies are also given, *E*(2).

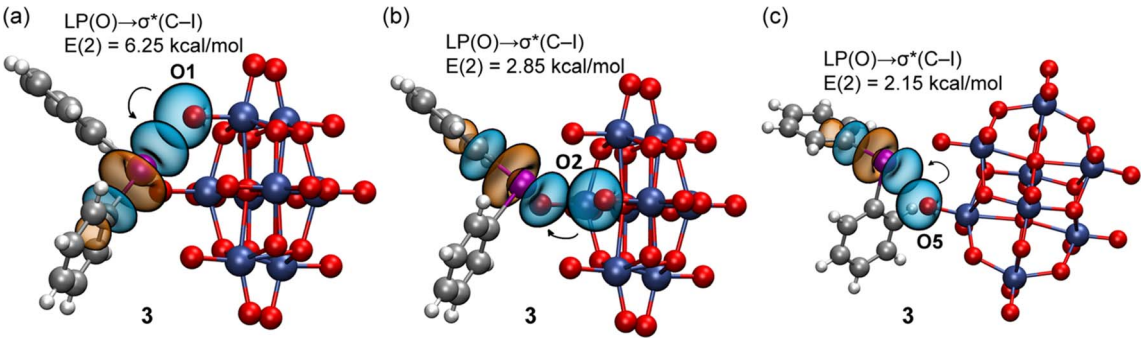

Fig. 11 NBOs involved in the XBs observed in **3** for the tetragonal pyramidal (a and b) and three-center (c) binding modes. The second order perturbation analysis energies are also given, *E*(2).

supramolecular assembly could also be achieved using other powerful σ-hole donors. Furthermore, this "key-to-lock" binding could be applied to various lacunary POMs such as, for instance, $[H_3PW_{11}O_{39}]^{4-}$ (ref. 97) or $[\gamma\text{-}SiW_{10}O_{34}(H_2O)_2]^{4-}$ (ref. 98–101) and also other double-σ-hole donors such as, for instance, the chalcogen bond donating compounds $R_2{}^{EWG}Ch$ (Ch = Se, Te).[102]

Secondly, examination of the occurrence of the XB-based tetragonal pyramidal moiety and analysis of appropriate NCIs provides an illustration of how different types of XB (namely, the two-center, bifurcated, and orthogonal XB; Fig. 4) could complement each other in the recognition system. The identification of the unusual orthogonal XB (which does not correspond to the IUPAC criteria for the recognition of XB) could be of interest for the crystal engineering community as this force might provide novel opportunities for targeted halogen-bond driven supramolecular assembly.

Finally, iodonium salts of $\alpha\text{-}[SiMo_{12}O_{40}]^{4-}$ and $[W_{10}O_{32}]^{4-}$ are applied as efficient initiators of radical photopolymerization of acrylates, cationic photopolymerization of epoxides, and photopolymerization of epoxy/acrylate blends.[88,89,103] These POMs are also used as POM-containing photocomposites exhibiting high catalytic activity toward photodecomposition (and decoloration) of dyes in aqueous solutions.[103] The achieved results of this study should be useful for the rational design of the iodonium-modified POM catalysts and final POM-based photocomposites. Works in this direction are underway in our group.

4. Experimental section

4.1. General information

$(n\text{-}Bu_4N)_4[\beta\text{-}Mo_8O_{26}]$[104] and the iodonium salts[91] were prepared according to the literature data. Other reagents were of commercial quality (Sigma-Aldrich) and were used without additional purification. Elemental analyses were carried out on a MICRO Cube CHN analyzer. IR spectra were recorded on a Bruker Vertex 60 FT-IR spectrometer (Section S8, the ESI†). Electrospray ionization (ESI) mass spectra were obtained on a Bruker maXis spectrometer equipped with an ESI source. The instrument was operated in positive ion mode using an *m*/*z* range 50–2600 (Section S9, the ESI†). The nebulizer gas flow was 0.4 bar, and the drying gas flow was 4.0 L min^{-1}.

4.2. Synthetic work and crystal growth

For details see Section S6, the ESI.†

4.3. X-ray single-crystal diffraction studies

Crystallographic data and refinement details are given in Table S2.† The diffraction data for **1**, **3**, and **4** were collected on a New Xcalibur (Agilent Technologies) diffractometer with MoKα radiation ($\lambda = 0.71073$) by doing φ scans of 0.5° frames at 150 K. Absorption correction was done empirically using SCALE3 ABSPACK (CrysAlisPro, Agilent Technologies, Version 1.171.37.35 (release 13-08-2014 CrysAlis171.NET)). The diffraction data for **2** and **5** were collected on a Bruker D8 Venture diffractometer with a CMOS PHOTON III detector and IμS 3.0 source (Mo Kα radiation, $\lambda = 0.71073$ Å) at 150 K. The φ- and ω-scan techniques were employed. Absorption correction was applied by SADABS (Bruker Apex3 software suite: Apex3, SADABS-2016/2 and SAINT, version 2018.7-2; Bruker AXS Inc.: Madison, WI, 2017). The structures were solved by SHELXT[105] and refined by full-matrix least-squares treatment against $|F|^2$ in anisotropic approximation with SHELX 2014/7 (ref. 106) in ShelXle program.[107] H-atoms were refined in geometrically calculated positions. In the crystal structure of **5**, DMSO molecules of crystallization demonstrate complicated orientation disorder with low occupancies. These molecules were treated by SQUEEZE procedure[108] of PLATON program.[109] This gives 74e per void which can be assigned as 1.7 DMSO per formula unit.

4.4. X-ray powder diffraction

X-ray powder diffraction patterns were measured on a Bruker D8 Advance diffractometer using LynxEye XE T discriminated CuKα radiation. Samples were layered on a flat plastic specimen holder. For details see Section S7, the ESI.†

4.5. Theoretical methods

The calculations reported herein were performed using the Turbomole 7.2 program.[110] The level of theory used for the calculations was PBE0 (ref. 111)-D3 (ref. 112)/def2-TZVP.[113,114] For iodine, this basis set includes effective core potentials (ECP) and takes into consideration relativistic effects for the inner electrons.[114] The MEP surface plots of the anions and cations were generated using the 0.001 a.u. isosurface and the same level of theory. The topological analysis of the electron density was carried out according to the quantum theory of atoms in molecules (QTAIM) and noncovalent interaction plot index (NCIplot) methods proposed by Bader[115] and W. Yang *et al.*,[116] respectively. For clarity, only intermolecular critical points were represented in the QTAIM analyses. Both were represented using the VMD program.[117] The individual XB energies were evaluated using the equations proposed by Bartashevich and Tsirelson[118] for XB and Espinosa *et al.*[119] for HB. The NBO analysis[120] was performed using the same level of theory and the NBO7.0 program.[121]

Data availability

Supplementary crystallographic data for this paper have been deposited at Cambridge Crystallographic Data Centre (CCDC 2334360–2334364) and can be obtained *via* **https://www.ccdc.cam.ac.uk/data_request/cif**. Other data available within the article or its ESI† and can be provided in raw format upon request.

Author contributions

Natalia S. Soldatova – methodology, investigation, funding acquisition, writing – original draft; Amirbek D. Radzhabov – investigation, formal analysis; Daniil M. Ivanov – conceptualization, methodology, data curation; Sergi Burguera – investigation, formal analysis; Antonio Frontera – methodology, resources, writing – original draft; Pavel A. Abramov – conceptualization, methodology, writing – original draft; Pavel S. Postnikov – conceptualization, methodology, supervision, writing – review & editing; Vadim Yu. Kukushkin – conceptualization, supervision, project administration, writing – review & editing.

Conflicts of interest

There are no conflicts of interest to declare.

Acknowledgements

This work was supported by the Russian Science Foundation, project 23-73-10091. P. A. A. thanks the Ministry of Science and Higher Education of the Russian Federation for the access SCXRD facilities of NIIC SB RAS. Authors are grateful to the Center for Chemical Analysis and Materials Research (Saint Petersburg State University) for the physicochemical measurements.

References

1 E. Persch, O. Dumele and F. Diederich, *Angew. Chem., Int. Ed.*, 2015, **54**, 3290–3327.
2 X. Wu, A. M. Gilchrist and P. A. Gale, *Chem*, 2020, **6**, 1296–1309.
3 L. Escobar and P. Ballester, *Chem. Rev.*, 2021, **121**, 2445–2514.
4 J. Pancholi and P. D. Beer, *Coord. Chem. Rev.*, 2020, **416**, 213281.
5 N. Biot and D. Bonifazi, *Coord. Chem. Rev.*, 2020, **413**, 213243.
6 X. Zhang, Z. An, J. An and X. Tian, *Coord. Chem. Rev.*, 2024, **502**, 215601.
7 Y. Fan, J. He, S. Guo and H. Jiang, *ChemPlusChem*, 2024, e202300536.
8 B. B. Patnaik, S. Baliarsingh, A. Sarkar, A. S. S. Hameed, Y. S. Lee, Y. H. Jo, Y. S. Han and J. Mohanty, *Rev. Aquac.*, 2024, **16**, 190–233.
9 *Perspectives in Supramolecular Chemistry*, ed. J. Behr, Wiley, 1994, vol. 1.
10 I. Alkorta, J. Elguero and A. Frontera, *Crystals*, 2020, **10**, 180.
11 S. Scheiner, *J. Chem. Phys.*, 2020, **153**, 140901.
12 P. Molina, F. Zapata and A. Caballero, *Chem. Rev.*, 2017, **117**, 9907–9972.

13 A. S. Mahadevi and G. N. Sastry, *Chem. Rev.*, 2016, **116**, 2775–2825.
14 L. Brammer, A. Peuronen and T. M. Roseveare, *Acta Crystallogr., Sect. C: Struct. Chem.*, 2023, **79**, 204–216.
15 Y. Cornaton and J.-P. Djukic, *Acc. Chem. Res.*, 2021, **54**, 3828–3840.
16 G. Resnati and P. Metrangolo, *Coord. Chem. Rev.*, 2020, **420**, 213409.
17 M. Savastano, *Dalton Trans.*, 2024, **53**, 1373–1392.
18 H. Schneider, *J. Phys. Org. Chem.*, 2022, **35**, e4340.
19 N. N. Nguyen, R. Berger, M. Wagner, J. Thiel, H.-J. Butt and R. Graf, *J. Phys. Chem. C*, 2021, **125**, 15751–15757.
20 M. I. S. Veríssimo, D. V. Evtuguin and M. T. S. R. Gomes, *Front. Chem.*, 2022, **10**, 840657.
21 N. I. Gumerova and A. Rompel, *Nat. Rev. Chem.*, 2018, **2**, 0112.
22 B. D'Cruz, M. O. Amin and E. Al-Hetlani, *Ind. Eng. Chem. Res.*, 2021, **60**, 10960–10977.
23 N. I. Gumerova and A. Rompel, *Chem. Soc. Rev.*, 2020, **49**, 7568–7601.
24 Y. Gao, M. Choudhari, G. K. Such and C. Ritchie, *Chem. Sci.*, 2022, **13**, 2510–2527.
25 B. Yu, X. Zhao, J. Ni and F. Yang, *ChemPhysMater*, 2023, **2**, 20–29.
26 Y. Zhang, J. Liu, S.-L. Li, Z.-M. Su and Y.-Q. Lan, *EnergyChem*, 2019, **1**, 100021.
27 M. R. Horn, A. Singh, S. Alomari, S. Goberna-Ferrón, R. Benages-Vilau, N. Chodankar, N. Motta, K. (Ken) Ostrikov, J. MacLeod, P. Sonar, P. Gomez-Romero and D. Dubal, *Energy Environ. Sci.*, 2021, **14**, 1652–1700.
28 F. M. B. Gusmão, D. Mladenović, K. Radinović, D. M. F. Santos and B. Šljukić, *Energies*, 2022, **15**, 9021.
29 H. Hu, L. Lian, X. Ji, W.-L. Zhao, H. Li, W. Chen, H. N. Miras and Y.-F. Song, *Coord. Chem. Rev.*, 2024, **503**, 215640.
30 T. Ma, R. Yan, X. Wu, M. Wang, B. Yin, S. Li, C. Cheng and A. Thomas, *Adv. Mater.*, 2024, **36**, 2310283.
31 L. Li, Y.-T. Yu, N.-N. Zhang, S.-H. Li, J.-G. Zeng, Y. Hua and H. Zhang, *Coord. Chem. Rev.*, 2024, **500**, 215526.
32 C. Wang, B. Wang, H. Yang, Y. Wan, H. Fang, W. Bao, W. Wang, N. Wang and Y. Lu, *Chem. Eng. J.*, 2024, **483**, 149143.
33 S. Li, Y. Zhou, N. Ma, J. Zhang, Z. Zheng, C. Streb and X. Chen, *Angew. Chem., Int. Ed.*, 2020, **59**, 8537–8540.
34 M. Zhu, S. Han, J. Liu, M. Tan, W. Wang, K. Suzuki, P. Yin, D. Xia and X. Fang, *Angew. Chem., Int. Ed.*, 2022, **61**, e202213910.
35 E. G. Ribó, N. L. Bell, D. Long and L. Cronin, *Angew. Chem., Int. Ed.*, 2022, **61**, e202201672.
36 M. T.-K. Ng, N. L. Bell, D.-L. Long and L. Cronin, *J. Am. Chem. Soc.*, 2021, **143**, 20059–20063.
37 S. She, W. Xuan, N. L. Bell, R. Pow, E. G. Ribo, Z. Sinclair, D.-L. Long and L. Cronin, *Chem. Sci.*, 2021, **12**, 2427–2432.
38 D. Li, X. Zhang, J. Lv, P. Cai, Y. Sun, C. Sun and S. Zheng, *Angew. Chem., Int. Ed.*, 2023, **62**, e202312706.
39 A. Jimbo, C. Li, K. Yonesato, T. Ushiyama, K. Yamaguchi and K. Suzuki, *Chem. Sci.*, 2023, **14**, 10280–10284.
40 V. I. Komlyagina, N. F. Romashev, V. V. Kokovkin, A. L. Gushchin, E. Benassi, M. N. Sokolov and P. A. Abramov, *Molecules*, 2022, **27**, 6961.
41 P. A. Abramov, V. Y. Komarov, D. A. Pischur, V. S. Sulyaeva, E. Benassi and M. N. Sokolov, *CrystEngComm*, 2021, **23**, 8527–8537.
42 P. A. Abramov, *J. Struct. Chem.*, 2022, **63**, 2068–2082.
43 V. V. Volchek, N. B. Kompankov, M. N. Sokolov and P. A. Abramov, *Molecules*, 2022, **27**, 8368.
44 A. V. Chupina, V. Shayapov, A. S. Novikov, V. V. Volchek, E. Benassi, P. A. Abramov and M. N. Sokolov, *Dalton Trans.*, 2020, **49**, 1522–1530.
45 Q. Wu, J. Wang, L. Zhang, A. Hong and J. Ren, *Angew. Chem.*, 2005, **117**, 4116–4120.
46 A. Tian, Y. Ning, Y. Yang, X. Hou, J. Ying, G. Liu, J. Zhang and X. Wang, *Dalton Trans.*, 2015, **44**, 16486–16493.
47 X.-Y. Wang, W.-C. Chen, K.-Z. Shao, X.-L. Wang, L. Zhao and Z.-M. Su, *Chem. Commun.*, 2021, **57**, 1042–1045.
48 N. N. Harmalkar, B. R. Srinivasan and S. N. Dhuri, *Z. Naturforsch., B: J. Chem. Sci.*, 2022, **77**, 245–252.
49 Y.-Q. Lan, J.-F. Ma, J. Yang, X.-H. Wang and Z.-M. Su, *Inorg. Chem.*, 2007, **46**, 8283–8290.
50 P. Bolle, H. Serier-Brault, A. Boulmier, M. Puget, C. Menet, O. Oms, J. Marrot, P. Mialane, A. Dolbecq and R. Dessapt, *Cryst. Growth Des.*, 2018, **18**, 7426–7434.
51 J. Ying, C. Sun, L. Jin, A. Tian and X. Wang, *CrystEngComm*, 2021, **23**, 5385–5396.
52 S. Yue, W. Song, S. Pan, D. Liu, C. Li, J. Zang, J. Nan and J. Gui, *Energy Fuels*, 2023, **37**, 8988–8998.
53 Q. Lu, J. Ying, A. Tian and X. Wang, *Inorg. Chem.*, 2023, **62**, 16617–16626.
54 S. Benz, A. I. Poblador-Bahamonde, N. Low-Ders and S. Matile, *Angew. Chem.*, 2018, **130**, 5506–5510.
55 Y. Zhao, Y. Cotelle, N. Sakai and S. Matile, *J. Am. Chem. Soc.*, 2016, **138**, 4270–4277.
56 A. Docker, A. J. Martínez Martínez, H. Kuhn and P. D. Beer, *Chem. Commun.*, 2022, **58**, 3318–3321.
57 G. R. Desiraju, P. S. Ho, L. Kloo, A. C. Legon, R. Marquardt, P. Metrangolo, P. Politzer, G. Resnati and K. Rissanen, *Pure Appl. Chem.*, 2013, **85**, 1711–1713.
58 B. K. Saha, R. V. P. Veluthaparambath and V. G. Krishna, *Chem.–Asian J.*, 2023, **18**, e202300067.
59 G. Cavallo, P. Metrangolo, R. Milani, T. Pilati, A. Priimagi, G. Resnati and G. Terraneo, *Chem. Rev.*, 2016, **116**, 2478–2601.
60 R. Tepper and U. S. Schubert, *Angew. Chem., Int. Ed.*, 2018, **57**, 6004–6016.
61 L. C. Gilday, S. W. Robinson, T. A. Barendt, M. J. Langton, B. R. Mullaney and P. D. Beer, *Chem. Rev.*, 2015, **115**, 7118–7195.
62 L. Catalano, G. Cavallo, P. Metrangolo, G. Resnati and G. Terraneo, in *Topics in Current Chemistry*, Springer Verlag, 2016, vol. 373, pp. 289–309.
63 A. J. Peloquin, S. C. Hill, H. D. Arman, C. D. McMillen, D. Rabinovich and W. T. Pennington, *J. Chem. Crystallogr.*, 2021, **52**, 62–72.

64 A. Mukherjee, S. Tothadi and G. R. Desiraju, *Acc. Chem. Res.*, 2014, **47**, 2514–2524.
65 D. M. Ivanov, A. S. Novikov, G. L. Starova, M. Haukka and V. Y. Kukushkin, *CrystEngComm*, 2016, **18**, 5278–5286.
66 C. B. Aakeröy, M. Baldrighi, J. Desper, P. Metrangolo and G. Resnati, *Chem.–Eur. J.*, 2013, **19**, 16240–16247.
67 G. Cavallo, J. S. Murray, P. Politzer, T. Pilati, M. Ursini and G. Resnati, *IUCrJ*, 2017, **4**, 411–419.
68 F. Heinen, E. Engelage, C. J. Cramer and S. M. Huber, *J. Am. Chem. Soc.*, 2020, **142**, 8633–8640.
69 R. L. Sutar and S. M. Huber, *ACS Catal.*, 2019, **9**, 9622–9639.
70 D. L. Reinhard, D. Kutzinski, M. Hatta, E. Engelage and S. M. Huber, *Synlett*, 2024, **35**, 209–214.
71 R. Robidas, D. L. Reinhard, C. Y. Legault and S. M. Huber, *Chem. Rec.*, 2021, **21**, 1912–1927.
72 N. S. Soldatova, P. S. Postnikov, D. M. Ivanov, O. V. Semyonov, O. S. Kukurina, O. Guselnikova, Y. Yamauchi, T. Wirth, V. V. Zhdankin, M. S. Yusubov, R. M. Gomila, A. Frontera, G. Resnati and V. Y. Kukushkin, *Chem. Sci.*, 2022, **13**, 5650–5658.
73 A. D. Radzhabov, A. I. Ledneva, N. S. Soldatova, I. I. Fedorova, D. M. Ivanov, A. A. Ivanov, M. S. Yusubov, V. Y. Kukushkin and P. S. Postnikov, *Int. J. Mol. Sci.*, 2023, **24**, 14642.
74 N. S. Soldatova, V. V. Suslonov, D. M. Ivanov, M. S. Yusubov, G. Resnati, P. S. Postnikov and V. Y. Kukushkin, *Cryst. Growth Des.*, 2023, **23**, 413–423.
75 E. Merritt and B. Olofsson, *Angew. Chem., Int. Ed.*, 2009, **48**, 9052–9070.
76 N. S. Soldatova, P. S. Postnikov, V. V. Suslonov, T. Y. Kissler, D. M. Ivanov, M. S. Yusubov, B. Galmés, A. Frontera and V. Y. Kukushkin, *Org. Chem. Front.*, 2020, **7**, 2230–2242.
77 J. Li, Y. Zhao, B. Huang, Y. Wang, Z. Xiong, B. Xiao, Y. Zhao, Z. Xiao and P. Wu, *J. Cluster Sci.*, 2022, **33**, 2375–2381.
78 P. Politzer, J. S. Murray and T. Clark, *Phys. Chem. Chem. Phys.*, 2013, **15**, 11178.
79 J. S. Murray, P. Lane and P. Politzer, *J. Mol. Model.*, 2009, **15**, 723–729.
80 H. Wang, W. Wang and W. J. Jin, *Chem. Rev.*, 2016, **116**, 5072–5104.
81 T. Clark, M. Hennemann, J. S. Murray and P. Politzer, *J. Mol. Model.*, 2007, **13**, 291–296.
82 L. Fotović, N. Bedeković and V. Stilinović, *Cryst. Growth Des.*, 2023, **23**, 3384–3392.
83 L.-S. Wang, Y. Lu, G. M. Ó. Máille, S. P. Anthony, D. Nolan and S. M. Draper, *Inorg. Chem.*, 2016, **55**, 9497–9500.
84 D. Kuriakose and M. R. Prathapachandra Kurup, *Inorg. Chim. Acta*, 2020, **505**, 119472.
85 D. Kuriakose and M. R. P. Kurup, *Polyhedron*, 2019, **170**, 749–761.
86 M. Oszajca, Ľ. Smrčok and W. Łasocha, *Acta Crystallogr., Sect. C: Cryst. Struct. Commun.*, 2013, **69**, 1367–1372.
87 P. Xiao, F. Dumur, M.-A. Tehfe, B. Graff, J. P. Fouassier, D. Gigmes and J. Lalevée, *Macromol. Chem. Phys.*, 2013, **214**, 1749–1755.
88 P. Xiao, C. Simonnet-Jégat, F. Dumur, G. Schrodj, M.-A. Tehfe, J. P. Fouassier, D. Gigmes and J. Lalevée, *Polym. Chem.*, 2013, **4**, 4526.
89 H. Mokbel, P. Xiao, C. Simonnet-Jégat, F. Dumur, D. Gigmes, J. Toufaily, T. Hamieh, J. P. Fouassier and J. Lalevée, *J. Polym. Sci., Part A: Polym. Chem.*, 2015, **53**, 981–989.
90 F. Dumur, *Eur. Polym. J.*, 2023, **195**, 112193.
91 N. Soldatova, P. Postnikov, O. Kukurina, V. V. V. Zhdankin, A. Yoshimura, T. Wirth and M. S. Yusubov, *Beilstein J. Org. Chem.*, 2018, **14**, 849–855.
92 I. S. Aliyarova, D. M. Ivanov, N. S. Soldatova, A. S. Novikov, P. S. Postnikov, M. S. Yusubov and V. Y. Kukushkin, *Cryst. Growth Des.*, 2021, **21**, 1136–1147.
93 I. I. Fedorova, N. S. Soldatova, D. M. Ivanov, K. Nikiforova, I. S. Aliyarova, M. S. Yusubov, P. M. Tolstoy, R. M. Gomila, A. Frontera, V. Y. Kukushkin, P. S. Postnikov and G. Resnati, *Cryst. Growth Des.*, 2023, **23**, 2661–2674.
94 E. Arunan, G. R. Desiraju, R. A. Klein, J. Sadlej, S. Scheiner, I. Alkorta, D. C. Clary, R. H. Crabtree, J. J. Dannenberg, P. Hobza, H. G. Kjaergaard, A. C. Legon, B. Mennucci and D. J. Nesbitt, *Pure Appl. Chem.*, 2011, **83**, 1637–1641.
95 D. D. DesMarteau, W. T. Pennington, V. Montanari, B. H. Thomas and J. Fluor, *Chem*, 2003, **122**, 57–61.
96 G. Wu, P. J. Zheng, S. Z. Zhu and Q. Y. Chen, *Acta Crystallogr., Sect. C: Cryst. Struct. Commun.*, 1991, **47**, 1227–1230.
97 E. Radkov and R. H. Beer, *Polyhedron*, 1995, **14**, 2139–2143.
98 K. Kamata, M. Kotani, K. Yamaguchi, S. Hikichi and N. Mizuno, *Chem.–Eur. J.*, 2007, **13**, 639–648.
99 K. Kamata, Y. Nakagawa, K. Yamaguchi and N. Mizuno, *J. Catal.*, 2004, **224**, 224–228.
100 T. Hirano, K. Uehara, K. Kamata and N. Mizuno, *J. Am. Chem. Soc.*, 2012, **134**, 6425–6433.
101 V. Y. Evtushok, V. A. Lopatkin, O. Y. Podyacheva and O. A. Kholdeeva, *Catalysts*, 2022, **12**, 472.
102 A. V. Rozhkov, E. A. Katlenok, M. V. Zhmykhova, A. Y. Ivanov, M. L. Kuznetsov, N. A. Bokach and V. Y. Kukushkin, *J. Am. Chem. Soc.*, 2021, **143**, 15701–15710.
103 M. Ghali, C. Brahmi, M. Benltifa, C. Vaulot, A. Airoudj, P. Fioux, F. Dumur, C. Simonnet-Jégat, F. Morlet-Savary, S. Jellali, L. Bousselmi and J. Lalevée, *J. Polym. Sci.*, 2021, **59**, 153–169.
104 W. G. Klemperer, *Inorganic syntheses*, 1990, pp. 74–85.
105 G. M. Sheldrick, *Acta Crystallogr., Sect. A: Found. Adv.*, 2015, **71**, 3–8.
106 G. M. Sheldrick, *Acta Crystallogr., Sect. C: Struct. Chem.*, 2015, **71**, 3–8.
107 C. B. Hübschle, G. M. Sheldrick and B. Dittrich, *J. Appl. Crystallogr.*, 2011, **44**, 1281–1284.
108 A. L. Spek, *Acta Crystallogr., Sect. C: Struct. Chem.*, 2015, **71**, 9–18.
109 A. L. Spek, *Acta Crystallogr., Sect. D: Biol. Crystallogr.*, 2009, **65**, 148–155.
110 R. Ahlrichs, M. Bär, M. Häser, H. Horn and C. Kölmel, *Chem. Phys. Lett.*, 1989, **162**, 165–169.

111 C. Adamo and V. Barone, *J. Chem. Phys.*, 1999, **110**, 6158–6170.
112 S. Grimme, J. Antony, S. Ehrlich and H. Krieg, *J. Chem. Phys.*, 2010, **132**, 154104.
113 F. Weigend and R. Ahlrichs, *Phys. Chem. Chem. Phys.*, 2005, **7**, 3297.
114 F. Weigend, *Phys. Chem. Chem. Phys.*, 2006, **8**, 1057.
115 R. F. W. Bader, *Chem. Rev.*, 1991, **91**, 893–928.
116 J. Contreras-García, E. R. Johnson, S. Keinan, R. Chaudret, J.-P. Piquemal, D. N. Beratan and W. Yang, *J. Chem. Theory Comput.*, 2011, **7**, 625–632.
117 W. Humphrey, A. Dalke and K. Schulten, *J. Mol. Graphics*, 1996, **14**, 33–38.
118 E. V Bartashevich and V. G. Tsirelson, *Russ. Chem. Rev.*, 2014, **83**, 1181–1203.
119 E. Espinosa, E. Molins and C. Lecomte, *Chem. Phys. Lett.*, 1998, **285**, 170–173.
120 E. D. Glendening, C. R. Landis and F. Weinhold, *J. Comput. Chem.*, 2019, **40**, 2234–2241.
121 E. D. Glendening, J. K. Badenhoop, A. E. Reed, J. E. Carpenter, J. A. Bohmann, C. M. Morales, P. Karafiloglou, C. R. Landis and F. Weinhold, *Theor. Chem. Institute*, Univ. Wisconsin, Madison, WI, 2018.